IEICE TRANS. INF. & SYST., VOL.E94–D, NO.5 MAY 2011

PAPER

An Image Stabilization Technology for Digital Still Camera Based on Blind Deconvolution

Haruo HATANAKA[†a)], ***Member***, **Shimpei FUKUMOTO**[†], **Haruhiko MURATA**[†], ***Nonmembers***, **Hiroshi KANO**[††], ***Member***, ***and*** **Kunihiro CHIHARA**[†††], ***Fellow***

SUMMARY In this article, we present a new image-stabilization technology for still images based on blind deconvolution and introduce it to a consumer digital still camera. This technology consists of three features: (1) double-exposure-based PSF detection, (2) efficient image deblurring filter, and (3) edge-based ringing reduction. Without deteriorating the deblurring performance, the new technology allows us to reduce processing time and ringing artifacts, both of which are common problems in image deconvolution.

key words: *image stabilization, blind deconvolution, deblurr, point spread function, ringing reduction, digital still camera*

1. Introduction

A number of studies on image deconvolution have been conducted in the past few years [1]. Lately, some of them have been proposed to address hand-blur in digital still cameras [4], [5], [7], [8], [10]. It is unpractical, however, to apply them to a consumer digital camera because those image deconvolution algorithms require precise blur detection and long processing time and generate ringing.

We have developed a new image stabilization technology for a digital still camera based on blind deconvolution. This new technology reduces both processing time and ringing artifacts. In this article, we will first describe our newly developed image stabilization algorithm and the image stabilization system in which the algorithm has been implemented. Then, we will present some experimental results of this algorithm and system.

2. Previous Work

There are two processing steps in blind deconvolution. The first step is to estimate the point spread function (PSF) caused by camera motion, equivalent to the blurring kernel. The second step is to create the deblurred image by using the PSF.

Manuscript received July 20, 2010.
Manuscript revised January 8, 2011.

[†]The authors are with SANYO Electric Co., Ltd., Daito-shi, 574–8534 Japan.
[††]The author is with Kyoto Sangyo University, Kyoto-shi, 603–8555 Japan.
[†††]The author is with Nara Institute of Science and Technology, Ikoma-shi, 630–0101 Japan.
a) E-mail: haruo.hatanaka@sanyo.com

DOI: 10.1587/transinf.E94.D.1082

2.1 PSF Estimation

Cannon [2], Yitzhaky [3], Tanaka [4], and Moghaddam [5] proposed PSF-estimation algorithms based on the assumption that blur motions are linear and constant; however, this assumption may not lead to satisfactory estimates and correction results because the PSFs caused by actual hand-blur are often much more complicated. Ayers [6], Fergus [7], and Shan [8] have also proposed algorithms that assess PSF with complex shapes, but Ayers's algorithm is unstable and Fergus and Shan's propositions are time-consuming. Besides the algorithms mentioned above, there are other estimation algorithms using images with different exposure times, which are devised by Lim [9] and Yuan [10]. Yet, Lim's PSF estimates are inaccurate, and Yuan's method involves long iterations.

2.2 Image Deblurring

Richardson-Lucy [11], [12] and Wiener's algorithms [13] are commonly used as blur restoration techniques. Nevertheless, their algorithms share the same problem of intensifying ringing noise when attempting to improve the deblurring effectiveness. In addition, Richardson-Lucy's iterative approach is too time-consuming. Chalkov [14] proposed a new algorithm to reduce the ringing noise based on the edge strength of the deblurred image; however, the ringing noise still remains. Although the method proposed by Yuan [10] reduces the ringing noise by restoring a residual image from short- and long-exposure images, the ringing effect escalates even further if image subjects move while the two images are being taken.

3. Proposed Algorithm

The application of image deconvolution for image stabilization in a digital still camera has three challenges. First, the blur has to be estimated precisely without using gyro sensors. Second, the processing time has to be shortened. Third, the ringing artifacts in the deconvolved image need to be suppressed without compromising the effectiveness of deblurring. To solve these problems, we propose a new algorithm called *hand-blur refiner*, which consists of three distinctive functions as follows:

3.1 Double-Exposure-Based PSF Detector

3.1.1 Basic Algorithm

Image degradation caused by hand-blur is denoted by (1), where g and f represents the blurred image and blur-free image, respectively. h represents the blur kernel (PSF) and n represents the noise. The convolution operator is denoted by $\otimes$.

$$g(x,y) = f(x,y) \otimes h(x,y) + n \tag{1}$$

Equation (1) becomes (2) when it comes to the frequency domain. Here, G, F, H, and N are the Fourier transforms of g, f, h, and n, respectively.

$$G(u,v) = F(u,v) \cdot H(u,v) + N \tag{2}$$

There are several methods to compute the estimate of h, which is denoted by $\hat{h}$, from g and f. The Wiener filter is optimal in the sense that Mean Square Error (MSE) between $\hat{h}$ and h is minimal. The Wiener filter theory defines $\hat{h}$ as in (3). Here, α is the regularization parameter and $*$ is the conjugate transpose matrix. *InvFT* denotes the inverse Fourier transform.

$$\hat{h}(x,y) = InvFT\left(\frac{G(u,v)\cdot F^*(u,v)}{|F(u,v)|^2 + \alpha}\right) \tag{3}$$

In a similar way, $\hat{f}$, the estimate of f, is calculated from g and h using (4). Here, β is another regularization parameter.

$$\hat{f}(x,y) = InvFT\left(\frac{G(u,v)\cdot H^*(u,v)}{|H(u,v)|^2 + \beta}\right) \tag{4}$$

Ayers [6] proposed a method for estimating a PSF generated by a motion blur from a single blurred image (Fig. 1). In this method, firstly, a random image is set as the initial estimate of the deblurred image f''. Next, from the deblurred image f'' and the blurred image g, a blur kernel h is calculated by (3). h is then corrected using (5) and (6). Then, a deblurred image f is created by using the blurred image g and the corrected PSF h'' using (4), and the deblurred image f'' is obtained by correcting f using (7) and (8). Here,

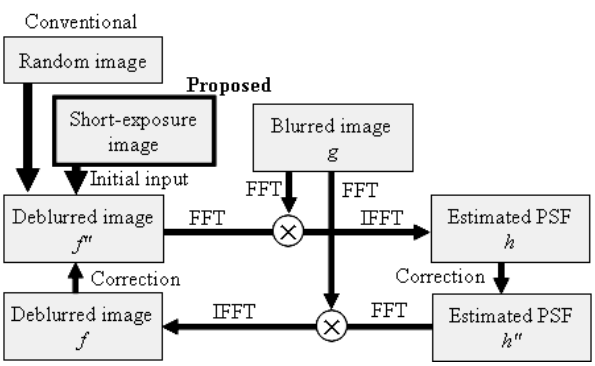

Fig. 1 Block diagram of Ayers' and proposed method.

$I_{\max}$ is a saturated pixel value of the output image. This process is repeated until the PSF converges, and after that, the estimate is finalized.

This method, however, has two drawbacks due to its iterative optimization procedure: (a) it requires a long processing time, and (b) it may be trapped by a local minimum, which will result in a wrong PSF.

$$h'(x,y) = \begin{cases} 1, & \text{if } h(x,y) > 1 \\ h(x,y), & \text{if } 0 \le h(x,y) \le 1 \\ 0, & \text{if } h(x,y) < 0 \end{cases} \tag{5}$$

$$h''(x,y) = \frac{h'(x,y)}{\sum h'(x,y)} \tag{6}$$

$$f'(x,y) = \begin{cases} I_{\max}, & \text{if } f(x,y) > I_{\max} \\ f(x,y), & \text{if } 0 \le f(x,y) \le I_{\max} \\ 0, & \text{if } f(x,y) < 0 \end{cases} \tag{7}$$

$$f''(x,y) = f'(x,y) \cdot \frac{\sum f(x,y)}{\sum f'(x,y)} \tag{8}$$

3.1.2 Proposed Method

To address these issues, we propose a new method that uses an image close to an ideal one without hand-blur as the initial estimate of the deblurred image instead of a random image (Fig. 1). First, two pictures are taken by pressing the shutter: one is a regular-exposure image, and the other is a short-exposure image. The exposure time for the latter is one that reportedly prevents hand-blur nearly perfectly. Specifically, it is set to 1/[focal length] (35-mm film equivalent). The signal gain of the short-exposure image is increased so that it can be equal to the regular-exposure image in average luminance. Next, the short-exposure image is set as the initial estimate of the deblurred image. Then, PSF h is calculated from the regular-exposure image g (blurred image) and the short-exposure image f'' (initial deblurred image) using (3). Then the same process as Ayers' method is repeated until the PSF converges. This method establishes an initial estimate of a deblurred image that is approximately equal to that of an ideal image without blur. Therefore, it results in an accurate estimate of PSF with fewer repeats and no local minimum.

However, it takes a long computation time to apply the above process to the entire image. To solve this problem, we select small regions with particular characteristics and estimate a unique PSF for them [15]. Specifically, we select four small patches of size 64 pixel by 64 pixel with high-edge strength from the short-exposure image and find each corresponding patch from the regular-exposure image by a block-matching method. The following m equations in (9) can be obtained by selecting m corresponding image patches.

$$g_i(x,y) = f_i(x,y) \otimes h(x,y) + n_i \quad (i = 1, \ldots, m) \tag{9}$$

Here, f_i represents the i-th image patch in the short-exposure image. g_i represents the corresponding image patch in the

regular-exposure image. h denotes the blur kernel, and n_i denotes noise. The m equations are transformed to the frequency domain and combined to obtain (10).

$$\begin{bmatrix} G_1(u,v) \\ G_2(u,v) \\ \cdots \\ G_m(u,v) \end{bmatrix} = \begin{bmatrix} F_1(u,v) \\ F_2(u,v) \\ \cdots \\ F_m(u,v) \end{bmatrix} H(u,v) + \begin{bmatrix} N_1 \\ N_2 \\ \cdots \\ N_m \end{bmatrix} \quad (10)$$

Here, G_i, F_i, and N_i are the Fourier transforms of g_i, f_i, and n_i, respectively. When $[G_1, G_2, \ldots, G_m]^T$, $[F_1, F_2, \ldots, F_m]^T$, and $[N_1, N_2, \ldots, N_m]^T$ are substituted with G, F, and N, respectively, Eq. (10) becomes (2). Therefore, $\hat{h}$, the estimate of the blur kernel h, is obtained by (3).

3.2 Efficient Image Deblurring Filter

If the estimated PSF does not have singular zero points, the complete deblurred image can be created by applying an inverse filter calculated from the blur kernel to the blurred image. However, the inverse filter obtained from the blur kernel is often singular and ill-posed. There are no clear and simple methods to determine the size and its coefficients of a deblur kernel (deconvolution filter). To address this issue, we propose a new algorithm to determine a small and effective deblur kernel. The algorithm includes the following two techniques:

3.2.1 Trimming of Deconvolution Filter Coefficients

Firstly, the deconvolution filter calculated by Wiener's method is trimmed by invalidating the coefficients which is less than a threshold using (11).

$$coeff(x,y) = \begin{cases} 0, & \text{if } |coeff(x,y)| \le threshold \\ coeff(x,y), & \text{otherwise} \end{cases} \quad (11)$$

A larger threshold results in a smaller filter size; however, the deblurring becomes less effective. Therefore, we optimized the threshold from experimental results shown in Fig. 2. Later, a pseudo-blurred image is created by applying a known PSF to a blur-free image, and the blurred image is deblurred while changing the threshold. The peak signal to noise ratio (PSNR) of the blur-free image and the deblurred image is then calculated to evaluate the result. A larger PSNR infers a better result as shown in Fig. 2. The optimal threshold is determined to be the point where PSNR begins to decrease rapidly. This technique achieves smaller deconvolution filter while maintaining PSNR.

3.2.2 Window Function

The second technique is to condense the deconvolution filter. Generally, applying a window function to a filter suppresses the ripples in the filter without altering the frequency response. Our method proposed in this article applies a hamming window (12), which is one of the representative window functions, to the deconvolution filter. Here, w represents the window function coefficient, d denotes the distance from the center of the filter, and D is the size of the filter. Figure 3 shows an example of applying a humming window to a one-dimensional deconvolution filter, indicating that the ripples on both ends of the filter are suppressed by the humming window. Therefore, this method can reduce the filter size while maintaining the filter characteristic (deblurring effectiveness).

$$w(d) = \begin{cases} 0.54 - 0.46\cos\left(\dfrac{\pi(2d+D)}{D}\right), & \text{if } -\dfrac{D}{2} \le d \le \dfrac{D}{2} \\ 0, & \text{otherwise} \end{cases} \quad (12)$$

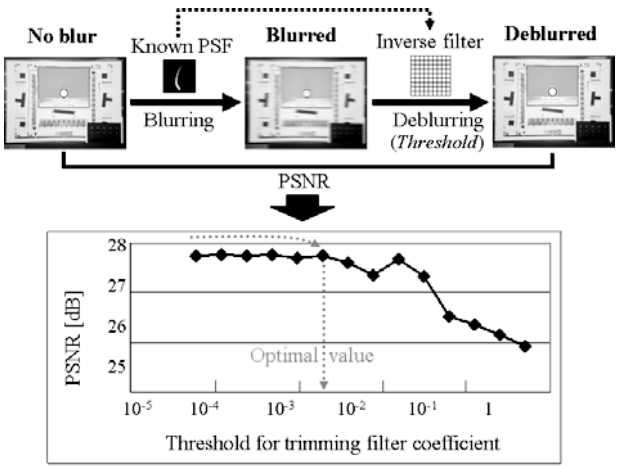

Fig. 2 Relationship between PSNR and threshold for trimming filter coefficients.

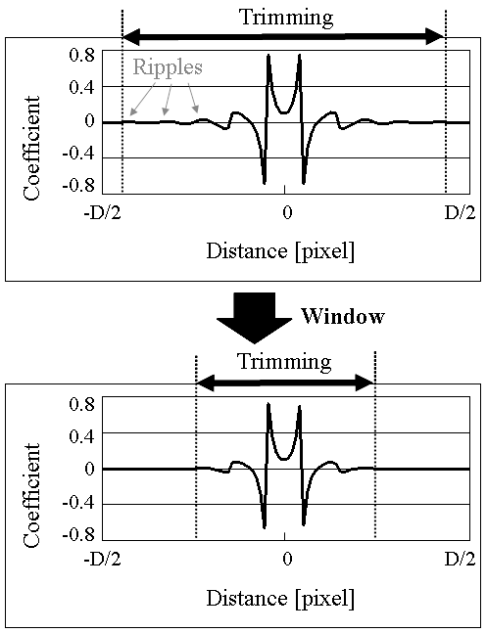

Fig. 3 Example of window function.

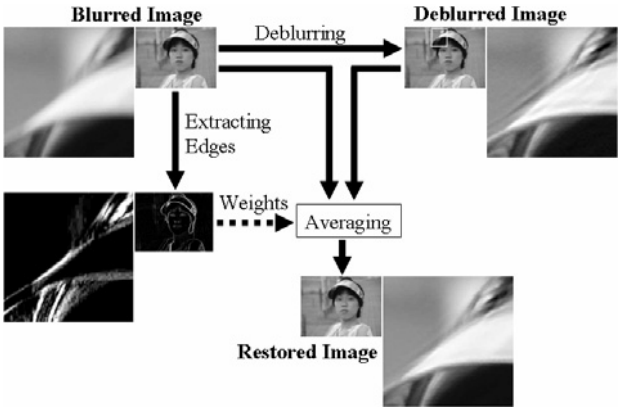

Fig. 4 Block diagram of edge-based ringing reduction.

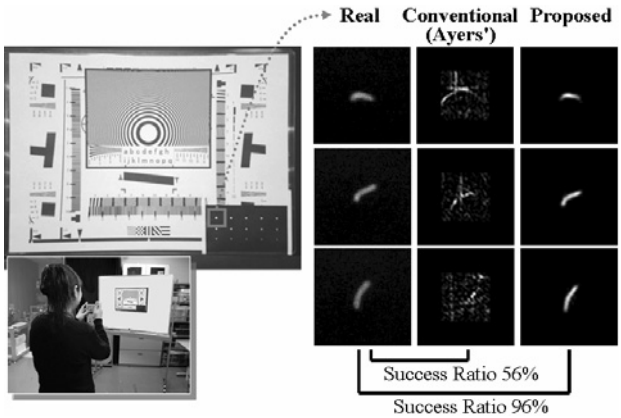

Fig. 5 Experiment of PSF estimation.

Table 1 Comparison between conventional and proposed methods.

	Conventional	Proposed
Success ratio	56 %	96 %
Processing time	30 s	0.3 s

Image size: 8 Mpixel, Exposure time: 1/15 s, PC: Pentium4 (3 GHz)

3.3 Edge-Based Ringing Reduction

As stated in "2. Previous Work," some approaches for inhibiting ringing noise have been proposed, but they all present an issue of reducing the deblurring effectiveness. To solve this problem, we propose a new method to reduce ringing using humans' visual characteristic without lowering the deblurring effect. The basic idea is that ringing is perceived from the low-frequency image areas, while deterioration due to hand-blur is perceived from the high-frequency image areas, so if we blend a blurred image and a deconvolved image using pixel-wise weights based on spatial frequency, we can effectively removes the ringing. Figure 4 shows the block diagram of our proposed method.

First, a deblurred image is generated from a blurred image using methods described earlier. Next, we generate an edge-extracted image by applying 3×3 Prewitt filter to the blurred image. Then, weighted-addition of the blurred and deblurred images is carried out on the basis of the weight of the pixel value of the edge-extracted image using (13), where r, b, d, and e, represents the restored image, blurred image, deblurred image, and edge-extracted image respectively. w represents the weight for addition. $e_{\max}$ and $e_{\min}$ denotes the maximum and minimum value of e. This method effectively removes ringing in the low-contrast area where ringing is noticeable as well as prevents reduction of sharpness, which is an indicator of the deblurring effect.

$$\begin{aligned} r(x,y) &= (1 - w(x,y)) \cdot b(x,y) + w(x,y) \cdot d(x,y) \\ w(x,y) &= \frac{e(x,y) - e_{\min}}{e_{\max} - e_{\min}} \end{aligned} \tag{13}$$

4. Experimental Results

We have evaluated the performance of the three methods of the *hand-blur refiner* using PC simulation.

4.1 Blur Detection Performance

Tests were conducted for images taken with an exposure time of 1/15 s and a focal length of 105 mm (35-mm equivalent) (Fig. 5). A panel-printed dotted pattern was placed in front of a resolution chart and 100 pictures of the chart were taken. Both Ayers' method and our double-exposure-based PSF detector were applied to the pictures. A comparison between the estimated PSFs and the real blur of the dotted pattern was conducted by evaluating the difference in shape and size. We defined the difference as D shown in (14), where h_1 and h_2 represents the estimated PSF and the real blur respectively. Dil and Bin denotes the 3×3 dilation and thresholding operation respectively. The PSF estimation was judged as a success if the difference D is 0. Table 1 shows their success ratios and processing times. Besides reducing the processing time by 100 times, we have improved the success ratio by 40 %.

$$\begin{aligned} D &= \sum_{D=0} \begin{cases} 1, & \text{if } \ Dil(h_1'(x,y)) < h_2'(x,y) \\ & \quad or\ Dil(h_2'(x,y)) < h_1'(x,y) \\ 0, & \text{otherwise} \end{cases}, \\ h'(x,y)_1 &= Bin(h_1(x,y)),\ h_2'(x,y) = Bin(h_2(x,y)) \end{aligned} \tag{14}$$

4.2 Deconvolution Performance

Blurred images were created by applying 20 different blur kernels to a blur-free image of the test chart and were deconvolved with both conventional and proposed deconvolution filters. Here, 512 pixel by 512 pixel filter size is employed for the conventional Wiener filter so as to maximize the deblurring performance. Proposed method 1 only applies the trimming technique while proposed method 2 applies both trimming and window function techniques. The processing time was measured via PC simulation and the PSNR values of each restored image and blur-free image pair were calculated respectively. Larger PSNR indicates better deblurring

result. The results are shown in Table 2. Compared to the conventional method, the proposed methods 1 and 2 on average requires shorter processing times by roughly a factor of 60 and 100, respectively, while maintaining similar PSNR values.

4.3 Ringing Reduction Performance

Figure 6 shows the experimental procedure to evaluate our ringing reduction method. The blurred images were created by applying 20 different blur kernels to a blur-free image of the test chart and were deconvolved with / without the proposed edge-based ringing reduction.

Figure 7 is an example of these images. We calculated each PSNR of the restored and the blur-free images. The results are shown in Table 3. Using our method, the average PSNR increased by 5 dB.

Table 2 Comparison between conventional and proposed methods.

	Conventional	Proposed 1 (Trimming)	Proposed 2 (Trimming +Window)
Deconvolution filter size	512 x 512 pixel	67 x 67 pixel	47 x 47 pixel
Processing time	2101 s	36 s	18 s
PSNR	27.8 dB	27.7 dB	27.6 dB

Image size: 8 Mpixel, Exposure time: 1/15 s, PC: Pentium4 (3 GHz)

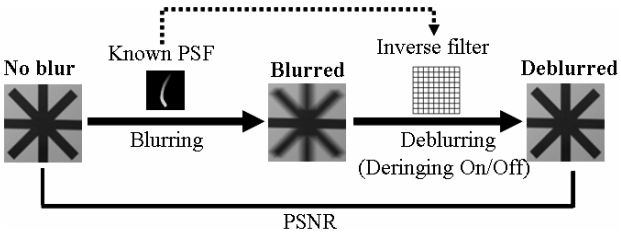

Fig. 6 Experimental procedure for our ringing reduction.

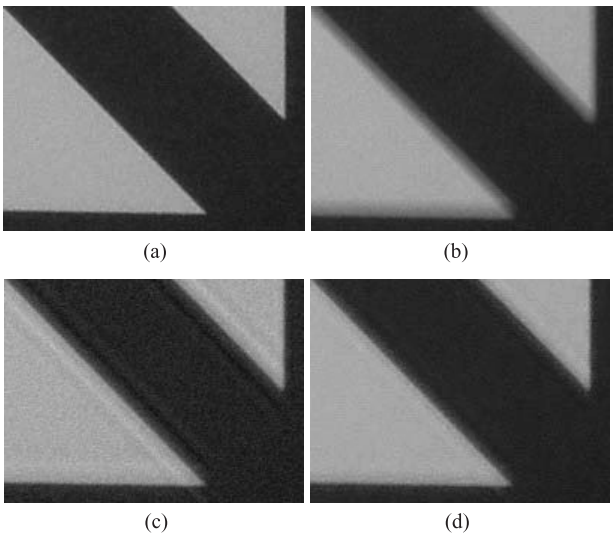

Fig. 7 Example images. (a) Blur-free image. (b) Blurred image. (c) Restored image without ringing reduction. (d) Restored image with ringing reduction.

Table 3 PSNR comparison between the two methods with and without ringing reduction.

	without ringing reduction	with ringing reduction
PSNR	27 dB	32 dB

Image size: 8 Mpixel, Exposure time: 1/15 s, PC: Pentium4 (3 GHz)

5. Prototype Camera

5.1 System Configuration

We have implemented the *hand-blur refiner* into a prototype digital still camera shown in Fig. 8.

Table 4 and Fig. 9 show the specifications and the block diagram of the camera system, respectively. Once the shutter button is pressed, both regular- and short-exposure images are taken and then loaded into the frame memory. After that, the Digital Signal Processing (DSP) estimates the PSF using both images, calculates the deconvolution filter coefficients, and sets up the Finite Impulse Response (FIR) filter. The FIR filter performs both filtering and deringing on the regular image and outputs the result to the LCD monitor as

Fig. 8 Prototype camera in which hand-blur refiner is implemented impimplemented.

Table 4 Specifications of the prototype camera.

Image sensor	1/2.5" CCD, 8 M pixel
Lens	3x Zoom
CPU	100 MHz
DSP	90 MHz / 16 bit fixed floating point
Frame memory	32 MB (3 MB for *hand-blur refiner*)

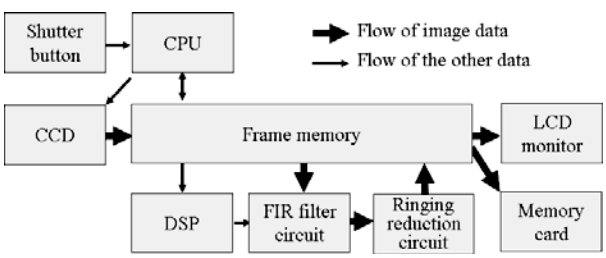

Fig. 9 Block diagram of hand-blur refiner.

well as the memory card.

5.2 Overall Performance

The total performance of image stabilization is evaluated using a prototype camera in which the *hand-blur refiner* is implemented. PSNR is not suitable for evaluating the performance of image stabilization in practice because the PSNR is greatly influenced by the accuracy of the image registration of the blur-free image and the restored image taken at different time. We proposed an original method for measuring the actual performance of image stabilization. In our method, the area of the region surrounded by the Modulation Transfer Function (MTF) curve, which indicates the sharpness of images, serves as an indicator of the degree of hand-blur. This is because at the time of shooting the larger the hand blur is, the smaller the area of MTF in the image will be (Fig. 10). As a subject, we use a circular zone plate (CZP) that enables us to measure the MTF in all directions.

Evaluation results of the system using this method are shown in Fig. 11. The filled diamond points indicate the MTF area values for real blurred images taken by the camera held in hand. The square points indicate the values for restored images. Each point indicates the averaged MTF area of 100 images of CZP taken with different exposure times. The curves are approximated by a quadratic function to fit these points. From these curves, exposure time T_B of the blurred image and exposure time T_R of the restored image are extracted, both of which correspond to the same area of MTF. Then, a gain of exposure time N [EV] is obtained using (15). This indicator tells how the deblurring effect can make the exposure time longer for shooting without hand-blur. A larger N will obtain a higher deblurring effect.

$$N = \log_2 (T_R/T_B) \tag{15}$$

Table 5 shows the results of calculating all points on the curves using the equation above. The gain of exposure time by our method was in the range from 0.7 EV to 1.4 EV. The process time for an 8-M image was 3.1 s on average and

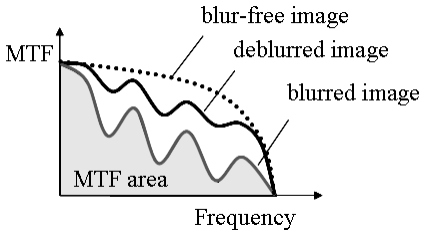

Fig. 10 MTF values for blurred and deblurred images.

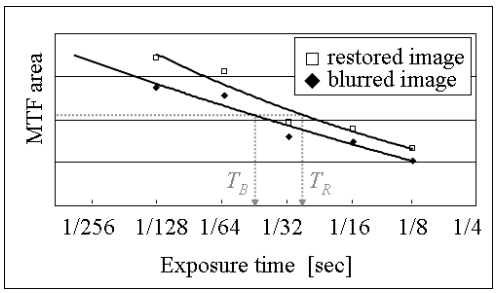

Fig. 11 Deblurring results for different exposures time.

Table 5 Total performance of our system.

Exposure time gain	0.7 – 1.4 EV
Processing time	Avg. 3.1 s (Max. 4.9 s)

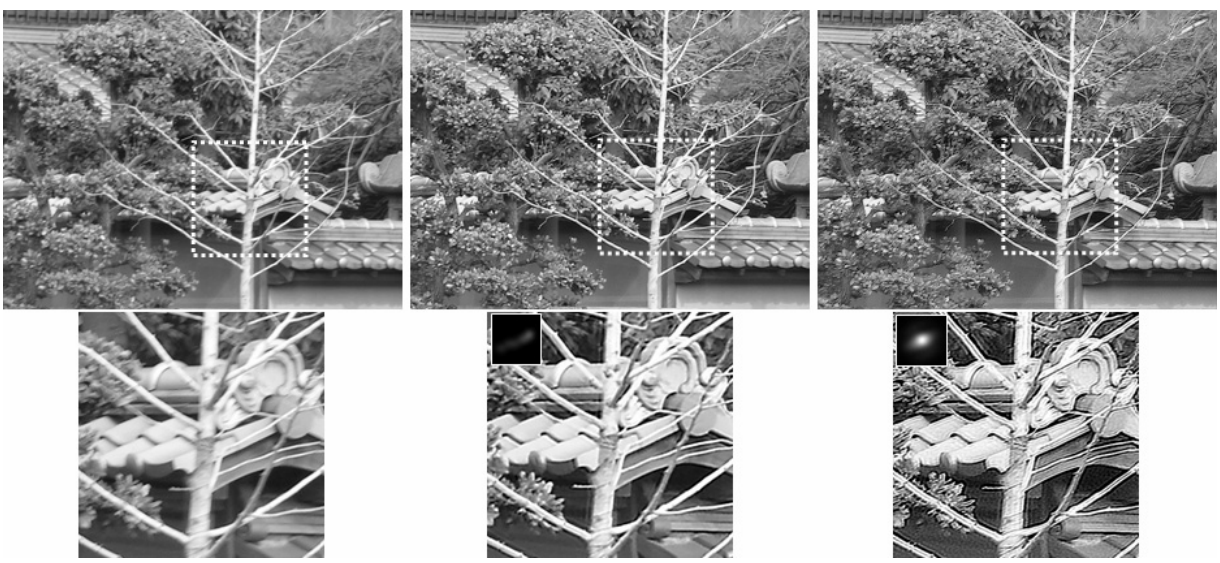

Fig. 12 Comparison of restored images. (a) Original image with hand-blur. (b) Restored image with hand-blur refiner. (c) Restored image with conventional method.

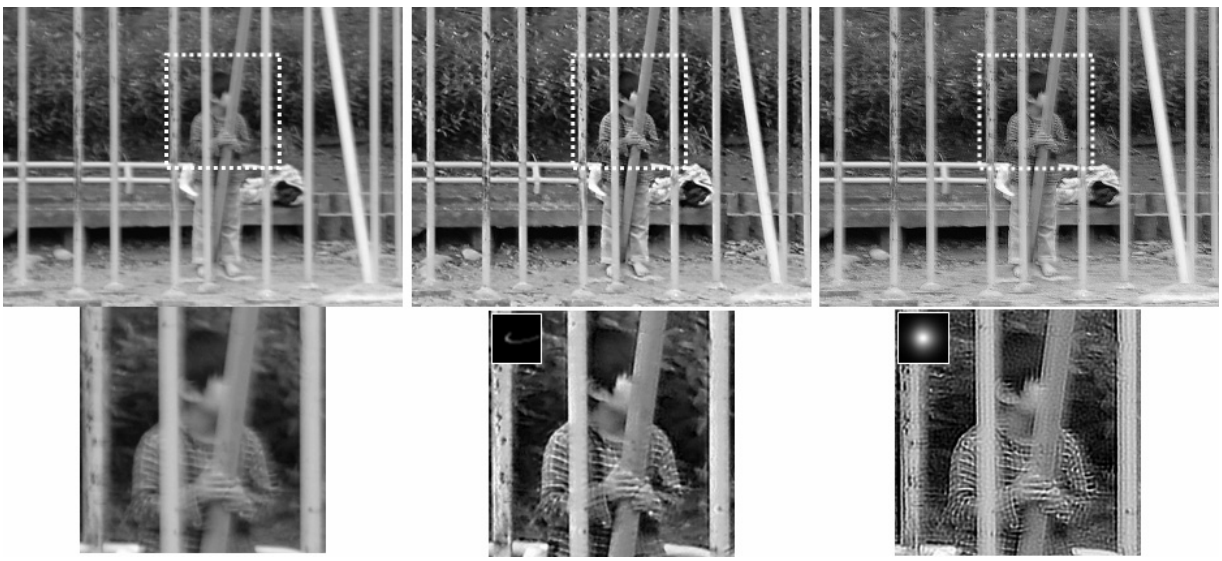

(a) (b) (c)

Fig. 13 Comparison of restored images. (a) Original image with hand-blur. (b) Restored image with *hand-blur refiner*. (c) Restored image with conventional method.

4.9 s at maximum.

Finally, we present a comparison between the restored images with the *hand-blur refiner* and a conventional blind deconvolution method, as shown in Fig. 12 and Fig. 13. The conventional method is based on an iterative procedure, known as the deconvblind function in MATLAB.

6. Conclusion

We have developed a new image stabilization technology based on blind deconvolution and successfully implemented it in a digital still camera. Evaluation results show that in the 1/125–1/8 s exposure time range we have achieved a 0.7–1.4 EV exposure time gain as well as reduced the processing time to 3 s on average.

Although we have proved that our technology can successfully perform in an actual digital camera, there is still room for improvement. One possibility is to remove the spatially-variant blur. To do that, a scheme that estimates blur kernels for small regions would be required. Another potential improvement is to reduce the shooting time for the second image. To achieve that, it would be effective to use a live preview image, right before pressing the shutter, instead of shooting the short-exposure image.

Moreover, the application of this algorithm in conjunction with optical hand-blur correction system can yield even better deblurring performance. Furthermore, our technology is applicable not only to image degradation by hand-blur but to image degradation by defocusing as well.

References

[1] M.R. Banham and A.K. Katsaggelos, "Digital image restoration," IEEE Signal Process. Mag., vol.14, no.2, pp.24–41, 1997.
[2] T.M. Cannon, "Blind deconvolution of spatially invariant image blurs with phase," IEEE Trans. Acoust. Speech Signal Process., vol.24, no.1, pp.58–63, 1976.
[3] Y. Yitzhaky, I. Mor, A. Lantzman, and N.S. Kopeika, "Direct method for restoration of motion-blurred images," J. Optical Society of America A, no.15, pp.1512–1529, 1998.
[4] M. Tanaka, K. Yoneji, and M. Okutomi, "Motion blur parameter identification from a linearly blurred image," IEEE International Conference on Consumer Electronics, 2007.
[5] M.E. Moghaddam and M. Jamzad, "Linear motion blur parameter estimation in noisy images using fuzzy sets and power spectrum," EURASIP Journal on Advances in Signal Processing, vol.10-1, 2007.
[6] G.R. Ayers and J.C. Dainty, "Iterative blind deconvolution method and its applications," Opt. Lett., vol.13, no.7, pp.547–549, July 1988.
[7] R. Fergus, B. Singh, A. Hertzmann, S.T. Roweis, and W.T. Freeman, "Removing camera shake from a single photograph," ACM Trans. Graphics, vol.25, no.3, pp.787–794, 2006.
[8] Q. Shan, J. Jia, and A. Agarwala, "High-quality motion deblurring from a single image," ACM Trans. Graphics, vol.27, no.3, Article 34, 2008.
[9] S.H. Lim and D.A. Silverstein, "Method for deblurring an image," US Patent Application, Pub. No. US2006/0187308 A1, Aug. 2006.
[10] L. Yuan, J. Sun, L. Quan, and H.-Y. Shum, "Image deblurring with blurred/noisy image pairs," ACM Trans. Graphics, vol.26, no.3, Article 1, 2007.
[11] W.H. Richardson, "Bayesian-based iterative method of image restoration," J. Optical Society of America, vol.62, pp.55–59, 1972.
[12] L.B. Lucy, "An iterative technique for the rectification of observed distributions," Astronomical J. vol.79, pp.745–754, 1974.
[13] N. Wiener, Extrapolation, Interpolation and Smoothing of Stationary Time Series with Engineering Applications, The MIT Press, 1964.
[14] S. Chalkov, N. Meshalkina, and C. Kim, "Post-processing algorithm for reducing ringing artifacts in deblurred images," 23rd International Technical Conference on Circuits/Systems, Computers and Communications, 2008.
[15] H. Kano, H. Hatanaka, S. Fukumoto, and H. Murata, "Motion blur estimation of handheld camera using regular- and short-exposure image pair," IEEE International Conference on Image Processing, 2009.

Haruo Hatanaka received his B.E. in mechanical system engineering from Hiroshima University, Japan in 1991. In the same year, he joined the R&D Headquarters of SANYO Electric Co., Ltd., to engage in research into the image processing technologies for digital cameras and video cameras. He is a manager at Audio and Image Processing Department in Digital Technology Research Center.

Shimpei Fukumoto received his B.E. in computer science and systems engineering from Kobe University, Japan in 1998., Then, he joined the R&D Headquarters of SANYO Electric Co., Ltd., where he has been researching on image processing technologies. He is a chief researcher at the Audio and Image Processing Department in Digital Technology Research Center.

Haruhiko Murata received his B.E. instrumentation engineering from Kobe University in 1984 and his Ph.D. in image processing engineering from the Nara Institute of Science and Technology in 2001. Since 1984, he has been engaged in research on image processing technologies, and he is currently a general manager at the Digital Technology Research Center in SANYO Electric Co., Ltd.

Hiroshi Kano received his BE, ME, and DE degrees in information engineering from Kyoto University in 1982, 1984, and 1998 respectively. From 1998 to 2010, he had been engaged in research on image processing and computer vision in SANYO Electric Co., Ltd.,, and he is currently a professor at the Kyoto Sangyo University, Japan.

Kunihiro Chihara received his BE, ME, and DE degrees in engineering science from Osaka University in 1968, 1970, and 1973 respectively. He is currently a professor at the Graduate School of Information Science, Nara Institute of Science and Technology (NAIST), Japan. His research interests include ubiquitous computing, virtual reality, and multimedia. He is a member of IEEE, ACM, JSUM, ISCIE, VRSJ, and JSMBE.